



Dynamic Instability Behaviour Prediction of Curved Shell Composite Structure Using Different Higher-Order Theories

Ankit Gangwar¹ · Ashish Kumar Sahu¹ · Vikash Kumar¹ · Nitin Sharma² · Murat Yaylaci³ · Subrata Kumar Panda¹

Received: 15 February 2024 / Revised: 31 March 2024 / Accepted: 7 April 2024
© Springer Nature Singapore Pte Ltd. 2024

Abstract

Purpose This research paper explores the dynamic instability behaviour of laminated curved shell composite structures under in-plane loading conditions.

Methods Two higher-order theories (nine and ten degrees of freedom at each node) are adopted to develop the composite mathematical model considering the in-plane loading conditions to compute the parametric instability based on the finite element (FE) discretization technique. The system's differential equations of motion are converted into a set of ordinary differential equations and addressed as an ordinary eigenvalue solution utilizing the Bolotin approach.

Results The precision and adaptability of the current model are confirmed by comparing the current outcomes with the existing solutions. The influence of numerous constraints of the laminated curved shell composite structure is investigated, such as different structural forms, thickness and aspect ratio, diversity in end condition, and static and dynamic load factors. Additionally, the compared outcomes (excitation frequency) between two different models (Model I and Model II) are varying from 0.93 to 34% under the static load factors (low to high range).

Conclusion The outcomes of the developed numerical models are carefully examined, compared and discussed. Model II responses are showing a higher side excitation frequency when compared to Model I due to the presence of stretching term in displacement kinematics. The excitation frequency increases due to a decrease in static load factor and an increase in curvature and aspect ratio.

Keywords Finite element · Curved shell · Dynamic instability · Excitation frequency

✉ Subrata Kumar Panda
call2subrat@gmail.com; pandask@nitrkl.ac.in

Ankit Gangwar
agangwar643@gmail.com

Ashish Kumar Sahu
ashishkumarsahu.davvis@gmail.com

Vikash Kumar
vikashkr050sagar@gmail.com

Nitin Sharma
nits.iiit@gmail.com

Murat Yaylaci
murat.yaylaci@erdogan.edu.tr

¹ Department of Mechanical Engineering, National Institute of Technology Rourkela, Rourkela, Sundergarh, Odisha 769008, India

² School of Mechanical Engineering, KIIT (Deemed to be University, Bhubaneswar, Odisha 751024, India

³ Department of Civil Engineering, Faculty of Engineering and Architecture, Recep Tayyip Erdogan University, 53100 Rize, Turkey

List of Symbols

$[B^b]$	Operator matrix for curvature
$[B^s]$	Operator matrix for higher order strain terms
df	Total system DOFs
E_k	Kinetic energy
E_p	Potential energy
(F)	Externally applied Force
F_s	Static constituent of F
F_t	Dynamic constituent of F
$[I]$	Identity matrix
$[j]$	Elemental stiffness matrix
$[K]$	Stiffness matrix
$[K_g]$	Global geometric stiffness matrix
$\{m\}$	Generalized field variable
$[N]$	Shape function
P_{cr}	Critical buckling load
(S)	Stress matrix
S_e	Strain energy
S_{ll}, S_{mm} and S_{nn}	Normal stress tensor

W	Work done
$[X]$	Thickness coordinate matrix
ξ_{lm}, ξ_{ln} and ξ_{mn}	Shear stress tensor
(ζ)	Strain vector
$[\Pi]$	Global mass coefficient matrix
Ω_e	Excitation frequency
μ_s	Static load factor
μ_d	Dynamic load factor

Introduction

Laminated composites are widely utilized in advanced and lightweight industries like defense, space, and airplanes to achieve the anticipated result for contemporary structural standards. It is a vital component of innovative technology and is perfect for a structurally high strength-to-weight ratio and specific elastic modulus. During their operating life, laminated structures are subjected to a variety of dynamic loading conditions. Hence, a thorough investigation is required to study the effect of dynamic instability/loading on the structural behavior of composite laminate.

Several studies have explored the dynamic characteristics of plates under various loadings using advanced numerical techniques. These investigations have provided valuable insights into the response of these materials, shedding light on their performance in different scenarios. The influence of stiffeners and loadings on the stiffened laminated composite plates was examined through the FE Analysis due to normal/shock blast waves. The research, verified through numerical simulations, specifically focused on the strain–time behavior [1]. Another study delved into the impact behaviour of laminates using the FE method. The findings revealed that the peak force experienced during low-velocity impact increased with the specimen's width, highlighting the importance of specimen geometry in impact studies [2]. Tanveer and Singh studied forced linear and nonlinear transient vibrations of rectangular plates under uniform loads. The work demonstrated a strong correlation between the natural linear frequencies of the plates and those determined through transient response analysis [3]. The dynamic behaviour of composite plates due to underwater explosions was investigated using FE Analysis and fluid–structure interaction by Wang et al. The research provided valuable insights into the elastic dynamic behavior of these plates in a challenging underwater environment [4]. Civalek studied the nonlinear dynamic response of rectangular laminated composite plates, modeling moderately thick plates using the first-order shear deformation theory (FSDT). This approach allowed for a comprehensive analysis of the plates' behavior under dynamic loads [5]. An innovative extension of the isogeometric technique was employed to analyze the dynamic response of laminated FG-CNTRC plates with piezoelectric

layers. This study utilizes the shear deformation theory of higher-order (HSDT) and explores the behavior of these advanced composite materials [6]. A Quasi 3-D theory along the plate's normal direction was proposed to study the laminated composite plate's free and forced vibration. This approach provided a practical and efficient means of analyzing their dynamic behaviour [7]. Gliszczyński et al. investigated the in-plane dimensional effects of fibre-reinforced laminated composites during low-velocity impact. Using 3D impact transient dynamic finite element analysis, the researchers presented the impact response for different aspect ratios, contributing to a better understanding of impact behavior in composite materials [8]. An expanded scaled boundary FE method (SBFEM) and precision integration technique (PIT) were used to examine the static responses of composite plates (electro-magneto). The study considered various boundary conditions and offered insights into the structural response of these plates [9]. The use of the fifth order shear deformation theory was employed to investigate the non-dimensional fundamental frequencies of glass fibre-reinforced laminated composite plates with graphene and fly ash fillers. The research demonstrated that these plates with fillers exhibited increased normal and shear strength compared to their non-laminated counterparts [10]. Collectively, these studies have significantly contributed to our understanding of the dynamic behavior of laminated composite plates under diverse loading conditions, providing valuable information for engineering applications and materials design.

A comprehensive exploration of the buckling behavior in the laminated plates has unveiled a range of critical insights. Researchers have examined various buckling factors, considering different boundary conditions and material properties. For instance, the influence of boundary conditions and ply stacking order on in-plane bending-induced buckling was investigated, revealing that thinner laminates are more susceptible to bend-twist coupling effects [11, 12]. Additionally, the study by Baba and Baltacı highlighted the role of cutout shapes and ply orientations in buckling behavior under in-plane compression load [13]. Meanwhile, anti-symmetric laminates and clamped boundaries enhanced buckling loads in E-glass/epoxy plates under axial compression [14]. Furthermore, post-buckling behavior was explored, showing minimal changes in scattering when transitioning from uniaxial to biaxial compression. Developing efficient finite element models and probabilistic methods has facilitated accurate buckling analysis, even in scenarios with randomly varying material properties [15]. Studies employing advanced theories and finite element analysis delved into post-buckling behavior and provided valuable insights into the response of composite plates under various loading conditions. Innovative approaches, such as probabilistic methods and isogeometric analysis, expanded our understanding

of buckling in these structures [16–18]. Lastly, the incorporation of advanced theories like hyperbolic tangent Shear deformation theory and 3D finite element modeling demonstrated their effectiveness in understanding buckling behavior, emphasizing the significance of factors such as CNT volume proportion [19, 20]. These studies contribute to a deeper understanding of buckling phenomena in laminated composite plates, addressing practical considerations for design and structural integrity.

Comprehensive research on dynamic instability in anisotropic laminated composite structures has provided valuable insights into the intricate interplay of critical factors affecting stability utilizing diverse methodologies such as FE and various analytical approaches. Notably, the analysis involving C0 nine-noded quadrilateral elements underscores the positive influence of aspect ratio on stability while cautioning against excess plate layers [21]. Ganapathi and Balamurugan [22] work highlights how increasing shell thickness and layer count can mitigate plate instability. Kumar's [23] findings emphasize the nuanced susceptibility to instability, contingent upon a multitude of system parameters. Additionally, the enhancement of dynamic stability in laminated plates under in-plane harmonic edge loading is explained by the addition of increased stiffeners. [24]. Fayaz and his coauthors [25] study unveil the shifting of instability zones to lesser frequencies with greater layer counts due to geometric nonlinearity. The nonlinear analysis indicates that heightened load magnitudes result in amplified vibration amplitudes and the displacement of unstable regions in thin laminated composites [26]. Meanwhile, Sahoo and Singh's secant function-based zigzag theory draws attention to the amplification of plate dynamic instability under growing dynamic loads [27]. Further investigations reveal increased orthotropy in cross-ply laminated plates augments excitation frequencies [28]. Moreover, the inverse Trigonometric zigzag theory and the HSDT, as applied by Sahoo and Singh [29] and Chattopadhyay and Radu [30], respectively, expand our understanding by demonstrating how dynamic and static load combinations can alter the scope of instability regions (IR), underscoring the complexity of composite plate dynamics under dynamic loads. Sahoo and his co-researchers investigated the dynamic responses of laminated/hybrid composite with or without damages and explored filler effects. The conventional theories have been modified to incorporate fillers and lamina orientation, observing changes in natural frequencies and structure stiffness. The study revealed decreased stiffness with increased crack severity. Graphene boosts strength, while fly ash enhances hardness but reduces strength [31–33]. Parida et al. explored graphene and fly-ash effects and reviewed/examined the static and dynamic responses of functionally graded or glass fibre-reinforced polymeric composite structure/beam using various shear deformation theories based on

finite element methods and nonlocal principles. The results suggest that graphene boosts strength and thermal stability, while flyash enhances hardness and impact resistance. Graphene-filled plates excel in strength, load transfer, and water resistance over flyash-filled ones [34–39]. The surface integrity has been examined in hard-turning functionally graded/laminate or metallic specimens with nano fluid-assisted minimum quantity lubrication. Experimental and predictive model validation, SEM analysis, and optimization via genetic algorithm highlight eco-friendly machining benefits and potential industrial applications [40–43]. Jena et al. reported the frequency responses, crack detection and severity estimation in structural applications of fibre reinforced polymeric composite beams/structures, experimentally and numerically using finite element or neuro-fuzzy hybrid techniques highlighting structural health monitoring and potential applications in diverse industries. The findings indicate that the mode shapes change due to the presence of damage, and frequency values decrease with deeper cracks [44–51]. Further, the static and dynamic responses of laminated/corrugated FGM plates are studied experimentally and analytically using Donnell's shell theory and energy approaches based on Hamilton's principle [52–57].

Several research investigations have been conducted in the past to assess the dynamic behaviour of flat composite structures. After reviewing the literature study, it is clear that the analysis relies heavily on lower-order mid-plane kinematics of flat plate structure and lacks experimental corroboration. Based on the research disparity, this study assesses the dynamic instability behaviour of curved composite shell panels first time using two different types of higher-order models. The appropriate parametric instability analysis is derived using isoparametric FE steps considering each node's nine and ten degrees of freedom (DOF). The differential equations of motion are transformed into a set of ordinary differential equations and solved as an ordinary eigenvalue solution using the Bolotin method. Finally, the effect of various geometrical shapes, aspects, curvature and thickness ratio, end conditions, and load factors on curved structures are analyzed using multiple instances and briefly addressed.

Mathematical Formulation

The curved shell panel having length ' a_1 ', width ' a_2 ' and thickness ' h ' is supposed to be oriented along l , m , and n -axis, respectively, as shown in Fig. 1. The shell panel is assumed to have ' k ' number of layers with curvature radius ' r_x ' and ' r_y ' along l and m -axis, respectively. The different geometrical shapes of the structure are obtained by varying curvature radii along l and m -axis, as shown in Fig. 2.

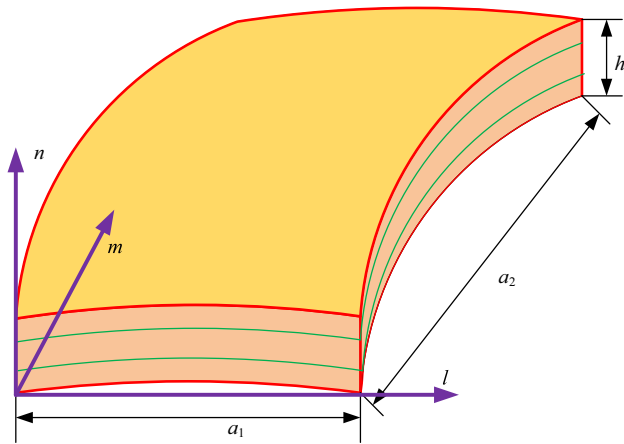


Fig. 1 Configuration of curved shell laminated structure

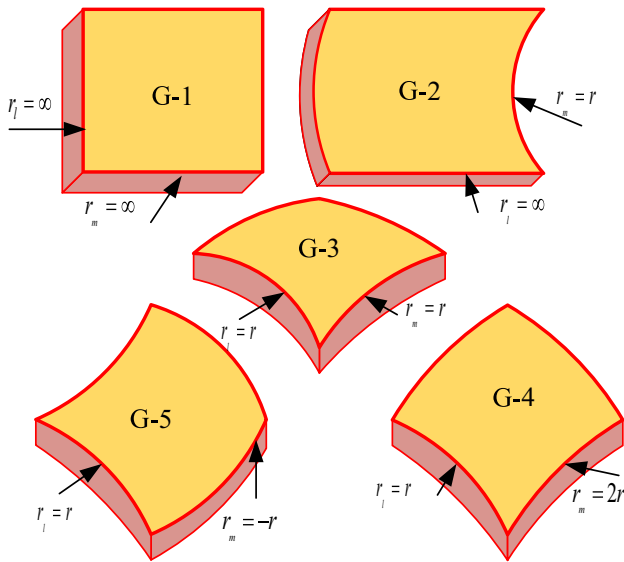


Fig. 2 Various forms of the structure

The kinematic displacement polynomial used in the present work are as:

Model I

$$\begin{aligned}
 V_{ll}(l, m, n, t) &= u_0(l, m, t) + n\theta_{ll}(l, m, t) + n^2\Lambda_{ll}(l, m, t) + n^3\Psi_{ll}(l, m, t) \\
 V_{mm}(l, m, n, t) &= v_0(l, m, t) + n\theta_{mm}(l, m, t) + n^2\Lambda_{mm}(l, m, t) + n^3\Psi_{mm}(l, m, t) \\
 V_{nn}(l, m, n, t) &= w_0(l, m, t)
 \end{aligned} \tag{1}$$

Model II

$$\begin{aligned}
 V_{ll}(l, m, n, t) &= u_0(l, m, t) + n\theta_{ll}(l, m, t) + n^2\Lambda_{ll}(l, m, t) + n^3\Psi_{ll}(l, m, t) \\
 V_{mm}(l, m, n, t) &= v_0(l, m, t) + n\theta_{mm}(l, m, t) + n^2\Lambda_{mm}(l, m, t) + n^3\Psi_{mm}(l, m, t) \\
 V_{nn}(l, m, n, t) &= w_0(l, m, t) + n\theta_{nn}(l, m, t)
 \end{aligned} \tag{2}$$

The global displacement of an arbitrary point along the $l, m,$ and n -directions is denoted by V_{ll}, V_{mm}, V_{nn} , respectively. The rotations of the transverse normal at the mid-plane along the l and m -axes are represented by θ_{mm} and θ_{ll} , respectively. Whereas θ_{nn} signifies the drilling degrees of freedom on the mid-plane. To accommodate the quadratic variation of shear strain, parameters $\Lambda_{ll}, \Lambda_{mm}, \Psi_{ll}, \Psi_{mm}$ are employed along the thickness of the structure.

$$\begin{pmatrix} S_{ll} \\ S_{mm} \\ S_{nn} \\ \xi_{lm} \\ \xi_{ln} \\ \xi_{mn} \end{pmatrix} = \begin{pmatrix} R_{11} & R_{12} & R_{13} & 0 & 0 & 0 \\ R_{21} & R_{22} & R_{23} & 0 & 0 & 0 \\ R_{31} & R_{32} & R_{33} & 0 & 0 & 0 \\ 0 & 0 & 0 & R_{66} & 0 & 0 \\ 0 & 0 & 0 & 0 & R_{55} & 0 \\ 0 & 0 & 0 & 0 & 0 & R_{44} \end{pmatrix} \begin{pmatrix} \zeta_{ll} \\ \zeta_{mm} \\ \zeta_{nn} \\ \zeta_{lm} \\ \zeta_{ln} \\ \zeta_{mn} \end{pmatrix} \tag{3}$$

or,

$$(S) = [\bar{R}](\zeta) \tag{4}$$

where $[\bar{R}]$ represents the transformed reduced stiffness matrix, and (S) denotes the stress matrix.

$$(\zeta) = \begin{pmatrix} \zeta_{ll} \\ \zeta_{mm} \\ \zeta_{nn} \\ \zeta_{lm} \\ \zeta_{ln} \\ \zeta_{mn} \end{pmatrix} = \begin{bmatrix} \frac{\partial V_{ll}}{\partial l} + \frac{V_{nn}}{Q_l} \\ \frac{\partial V_{mm}}{\partial m} + \frac{V_{nn}}{Q_m} \\ \frac{\partial V_{nn}}{\partial n} \\ \frac{\partial V_{ll}}{\partial m} + \frac{\partial V_{mm}}{\partial l} + \frac{2V_{nn}}{Q_{lm}} \\ \frac{\partial V_{ll}}{\partial n} + \frac{\partial V_{nn}}{\partial l} - \frac{V_{ll}}{Q_l} \\ \frac{\partial V_{ll}}{\partial n} + \frac{\partial V_{nn}}{\partial m} - \frac{V_{mm}}{Q_m} \end{bmatrix} \tag{5}$$

or,

$$(\zeta) = [X](\bar{\zeta}) \tag{6}$$

where $(\bar{\zeta})$ denotes strain vector and $[X]$ represents thickness coordinate matrix.

The vectorized expression for the externally applied forces can be formulated as follows:

$$(F) = [K](\zeta) \tag{7}$$

Furthermore, the components of the stiffness matrix can be articulated as follows:

$$[K] = \sum_{i=1}^n \int_{a_{i-1}}^{a_i} (\bar{R}_{ab})_i (1, s, s^2 \dots s^6) ds \tag{8}$$

The expression for the work done by the force {F} is formulated as follows:

$$W = \iint V^T(F) dldm \tag{9}$$

$$E_k = \frac{1}{2} \int_V \rho (\dot{V}_{ll}^2 + \dot{V}_{mm}^2 + \dot{V}_{nn}^2) dV \tag{10}$$

$$S_e = \frac{1}{2} \int_A (\{q\}^T [B^b]^T [D^b] [B^b] \{q\} + \{q\}^T [B^s]^T [D^s] [B^s] \{q\}) dA \tag{11}$$

where,

$$[D^b] = \sum_{c=1}^n \int_{x_c}^{x_{c+1}} [H^b]^T [Q_{ij}^b] [H^b] dx \quad \text{a n d} \tag{12}$$

$$[D^s] = \sum_{c=1}^n \int_{x_c}^{x_{c+1}} [H^s]^T [Q_{ij}^s] [H^s] dx.$$

The elemental stiffness is expressed as:

$$[j] = \int_A \left(\sum_1^n \int_{x_{c-1}}^{x_c} [H]^T [K] [H] dn \right) dA \tag{12}$$

where [H] denotes the strain–displacement matrix.

The differential equations (DE) governing the parametric stability examination of plates are derived using the Lagrangian equation, which is stated as follows:

$$\frac{d}{dt} \left(\frac{\partial E_k}{\partial \dot{m}} \right) + \frac{\partial S}{\partial m} - \frac{\partial E_p}{\partial m} = 0 \tag{13}$$

where, *m* is the general field variable. *E_k*, *S* and *E_p* denote the laminated composite plate's total kinetic energy, strain energy, and potential energy due to applied in-plane loading.

Now, by substituting the respective energy values in Eq. (13) and then carrying out the differentiation, the result is obtained as follows:

$$[\Pi] \{\ddot{m}\} + \{[K] - [K_g]\} \{m\} = 0 \tag{14}$$

w h e r e , $[\Pi] = \int_A [N]^T [I] [N] dA$, $[K_g] = \int_A ([B^b]^T [D^b] [B^b] + [B^s]^T [D^s] [B^s]) dA$

$$[K_g] = \int_A [B^s]^T [S^s] [B^s] dA \tag{15}$$

Now, the Eq. (14) can be rewritten by considering the in-plane load mechanisms as

$$[\Pi] \{\ddot{m}\} + \{[K] - (F_s + F_t \cos \Omega_e t) [K_g]\} \{m\} = 0 \tag{16}$$

where, *F_s* and *F_t* represents the static and dynamic constituent of *F*. *Ω_e* correspond to the excitation frequency.

The in-plane load comprises both static and dynamic components, which can be articulated with reference to the critical buckling load of a laminated composite plate as:

$$F_s = \mu_s P_{cr} \text{ and } F_t = \mu_d P_{cr} \tag{17}$$

where, *P_{cr}* represents the buckling load (critical) of the plate. *μ_d* and *μ_s* denote the dynamic and static load factors.

Now, by replacing Eq. (17) in Eq. (16), it becomes

$$[\Pi] \{\ddot{m}\} + \{[K] - \mu_s P_{cr} [K_g] - \mu_d P_{cr} \cos \Omega_e t [K_g]\} \{m\} = 0 \tag{18}$$

Now, Eq. (18) embodies a Mathieu-type ordinary DE, the solution of which delineates the instability features of the structure.

Equation (18) are expressed through two concurrent periodic Fourier series with periods T and 2 T ($T = \frac{2\pi}{\Omega_e}$) as given in Eqs. (19) and (20), respectively, as:

$$[F_t] = \sum_{i=1}^{\infty} \left[l_i \sin \frac{(2i-1)\Omega_e t}{2} + m_i \cos \frac{(2i-1)\Omega_e t}{2} \right] \tag{19}$$

$$[F_s] = \frac{1}{2} a_0 + \sum_{i=1}^{\infty} \left[l_i \sin \frac{(2i)\Omega_e t}{2} + m_i \cos \frac{(2i)\Omega_e t}{2} \right] \tag{20}$$

where *l_i* and *m_i* are the arbitrary constants.

The principal instability zone's first-order approximation is expressed as follows:

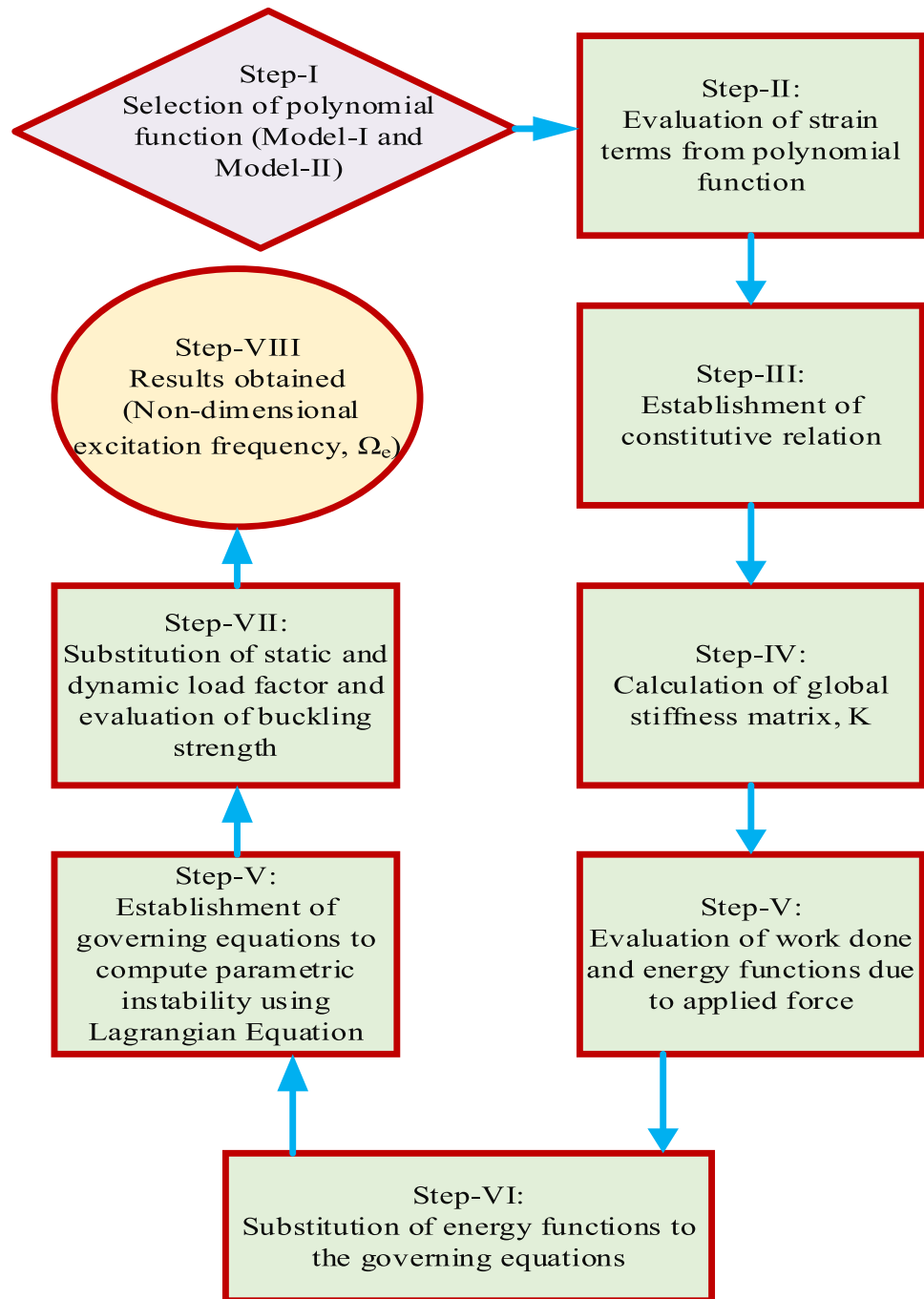
$$\left| \{[K] - \mu_s P_{cr} [K_g] \pm 0.5 \mu_d P_{cr} [K_g]\} - \frac{\Omega_e^2}{4} [\Pi] \right| = 0 \tag{21}$$

The maximum and minimum *Ω_e* is established by selecting the (+ve) and (-ve) sign one by one in the equation.

The subordinate IR can be obtained by determining the eigenvalue problem as $\{[K] - \mu_s P_{cr} [K_g]\} - \Omega_e^2 [M] = 0$.

$$\left| \begin{bmatrix} \{[K] - \mu_s P_{cr} [K_g]\} & -\mu_d P_{cr} [K_g] \\ -0.5 \mu_d P_{cr} [K_g] & \{[K] - \mu_s P_{cr} [K_g]\} \end{bmatrix} - \begin{bmatrix} [0]_{df \times df} & [0]_{df \times df} \\ [0]_{df \times df} & [\Pi] \end{bmatrix} \right| = 0 \tag{22}$$

Fig. 3 Flow chart of mathematical modelling steps

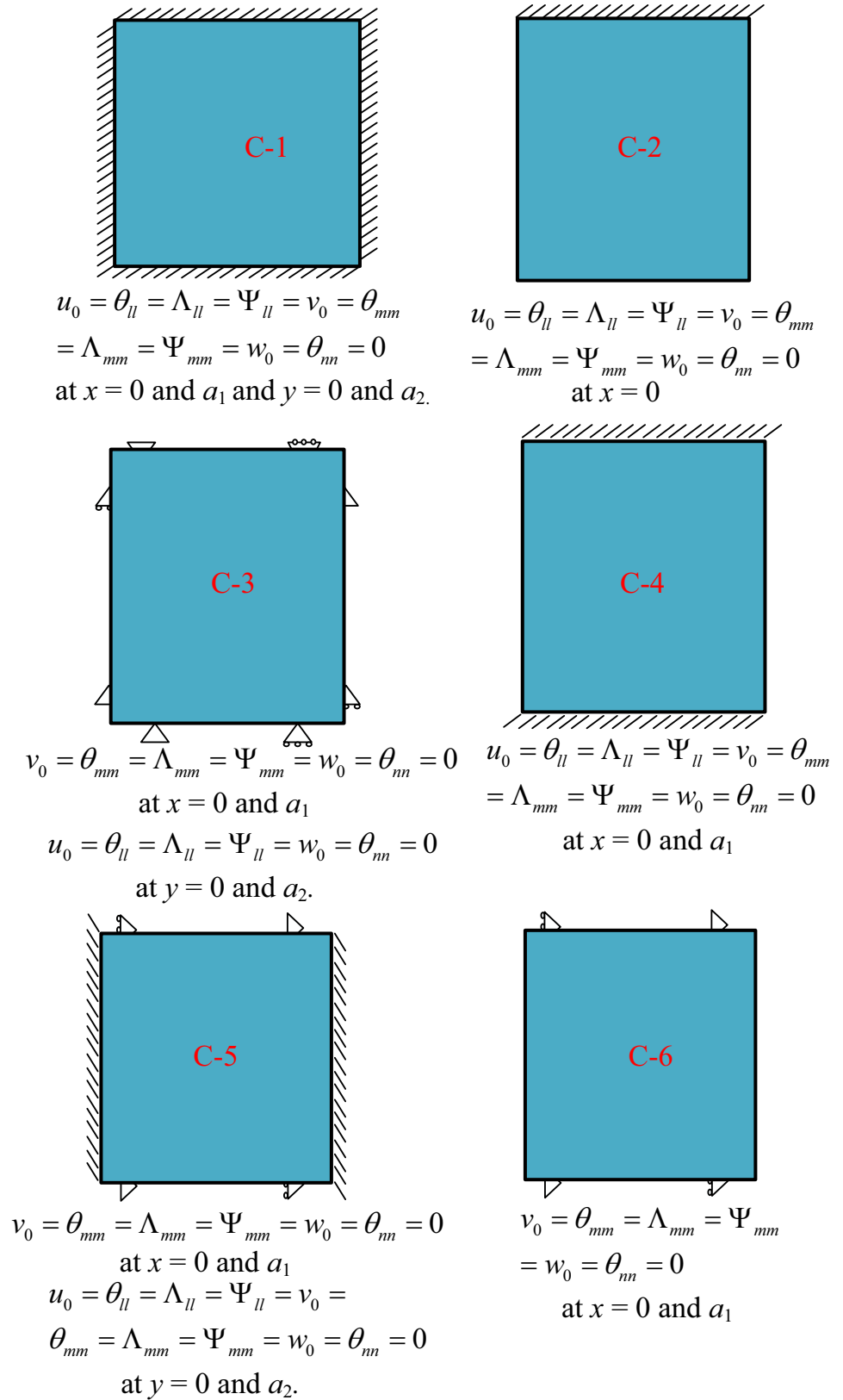


where df indicates the total system DOFs.

The detailed steps of mathematical modelling are also provided as a flow chart in Fig. 3. Figure 4 provides the specifics of the different constraints for each edge length to achieve different boundary conditions. The limitations are imposed along the edge length to diminish the number of unknowns and to obtain the solution of the laminated structural problems. In order to ensure stress continuity, the kinematic equation in the current

study includes ten variables: displacement (u_0 , v_0 , and w_0), rotation (θ_{ll} , θ_{mm} , θ_{nn}), and parabolic variation terms (Λ_{ll} , Λ_{mm} , Ψ_{ll} , Ψ_{mm}). Distinct edge lengths are restricted as per various specifics presented in Fig. 4 to achieve various end conditions.

Fig. 4 Details of boundary condition



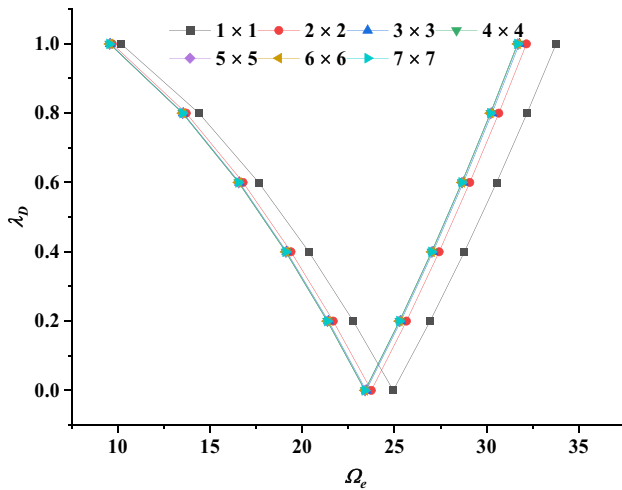


Fig. 5 Convergence behaviour of the laminated curved shell structure

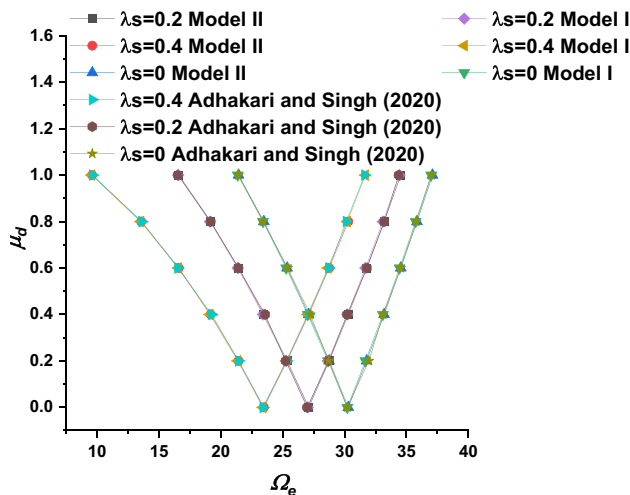


Fig. 6 Comparison of dynamic instability responses of flat plate structure using present developed Model I and II

Results and Discussion

Initially, a convergence test is used to ensure the consistency of the generated mathematical model. The non-dimensional excitation frequency (NDEF, Ω_e) response has been evaluated for various dynamic load factors (μ_d) and mesh densities, i.e., 1×1 , 2×2 , 3×3 , 4×4 , 5×5 , 6×6 , and 7×7 , considering simple support end condition and shown in Fig. 5. After a 4×4 mesh size, the output exhibits identical behaviour but computational time gets increased with mesh density. As a result, a 4×4 mesh size has been used throughout the investigation to study

the NDEF responses of curved shell structures without jeopardizing precision and processing time. The structural and material properties remain the same as: $a = 1$, $b = 1$, $al/h = 20$, layup sequence $[0/90]_4$, $E_{11}/E_{22} = 40$, $G_{12}/E_{22} = 0.6$, $G_{13}/E_{22} = 0.6$, $G_{23}/E_{22} = 0.5$, $\nu_{12} = 0.25$.

The NDEF responses of flat plate structures have been evaluated at various static and dynamic load factors. The outcomes are compared and presented in Fig. 6. The structural and material properties remain the same as ref. [7]. The graphical output demonstrates the exactness of the currently developed mathematical model.

New Illustrations

After checking the coherence and reliability of the model, the NDEF (Ω_e) responses have been evaluated by considering different geometrical input parameters of the curved shell panel. The various consequences have been observed by varying the static and dynamic load factors. The geometrical and elastic properties utilized remains same as: $a = 1$, $b = 1$, $al/h = 20$ layup sequence $[0/90]_4$, $E_{11}/E_{22} = 40$, $G_{12}/E_{22} = 0.6$, $G_{13}/E_{22} = 0.6$, $G_{23}/E_{22} = 0.5$, $\nu_{12} = 0.25$, $\rho = 1 \text{ kg/m}^3$.

Effect of Geometry

In this example, a variety of laminated shapes are meticulously examined. The various shapes are obtained by varying the curvature radii along l and m -axis as shown in Fig. 2. The NDEF responses are evaluated utilizing the C-3 end condition having geometrical parameters as: $a_1 = a_2 = 1$, $r/a_1 = 40$, $a_1/h = 20$ and $\mu_s = 0.1$. The excitation frequency responses at various dynamic load factor ' μ_d ' and at constant static load factor ' μ_s ' are evaluated considering Model I and II and plotted in Fig. 7a, b, respectively. The results, depicted in Fig. 7, exhibit the effect of various shapes of the geometry on excitation frequency. An intriguing observation is observed as the point of origin identified is slightly higher in Model II than in Model I for the different geometric shell structures. Also, the dynamic instability region is almost the same in Model I for the distinct shape of the structure, while it varies slightly in Model II. Model I slightly underestimates the excitation frequency values compared to Model II due to the negligence of some strain terms.

Effect of Curvature Ratio

The influences of various R/a_1 ratios have been analyzed of curved shell structure with C-3 end condition having geometrical parameters used as $a_1 = a_2 = 1$, $r/a_1 = 40$, $a_1/h = 20$ and $\mu_s = 0.1$. The excitation frequency responses of G-2 and G-3 shell structures for Model I and II at various dynamic load factors ' μ_d ' are evaluated and plotted in Figs. 8 and 9, respectively. Notably, a distinct trend is observed: as

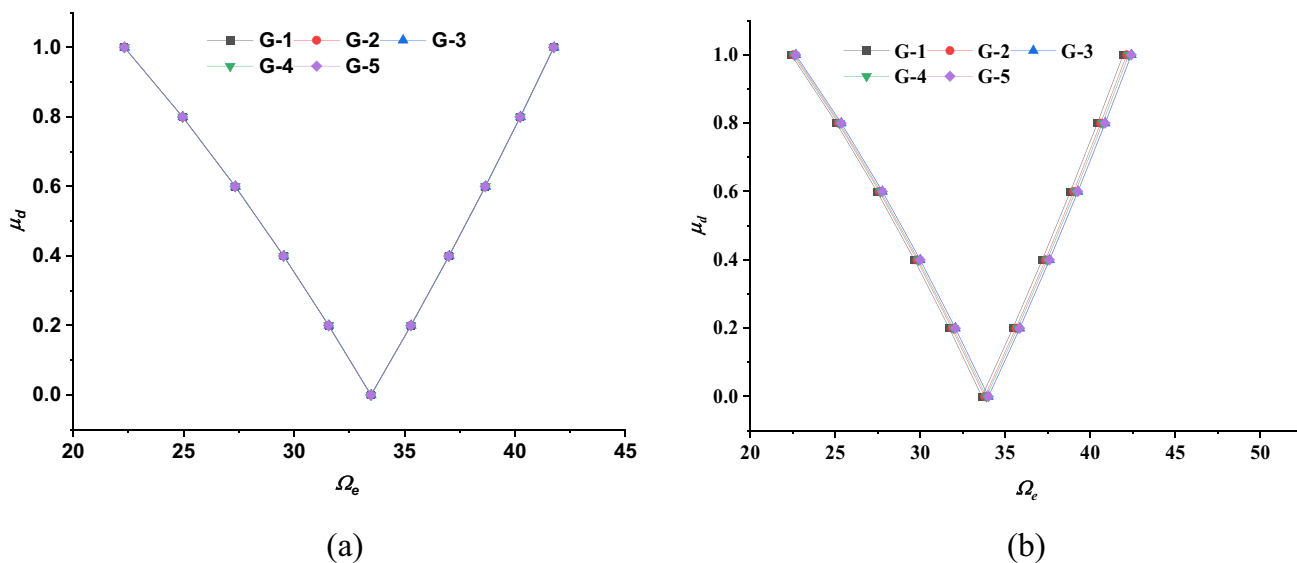


Fig. 7 Dynamic instability responses (DIR) of laminated shell panels $([0/90]_4)$ having $R/a=40$, $a/h=20$ and $\mu_s=0.1$ for different geometries a Model I b Model II

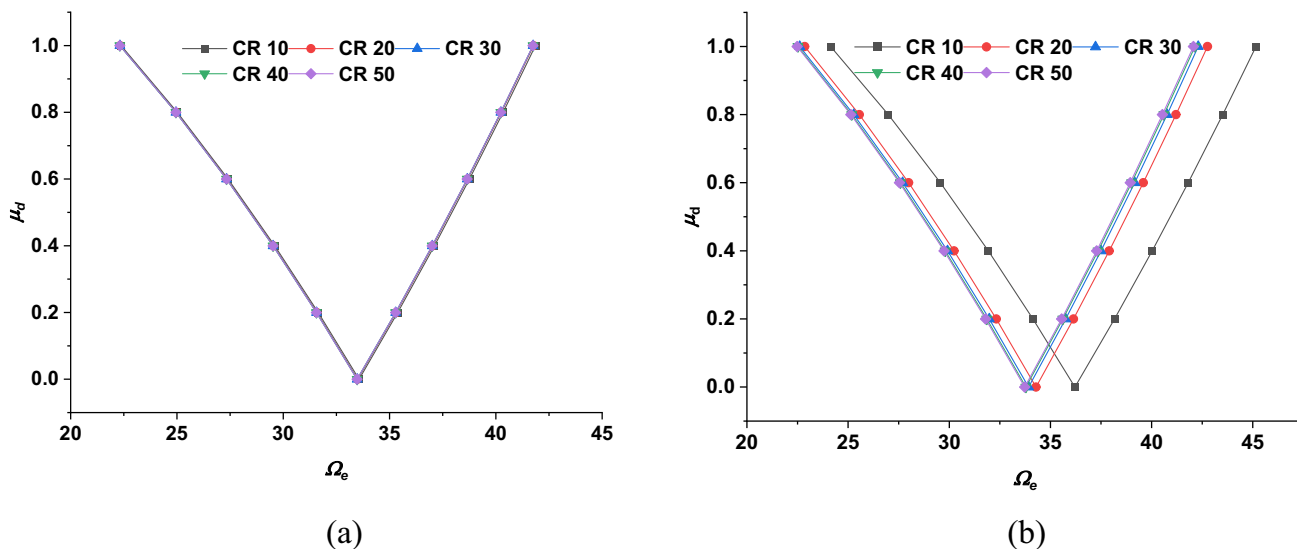


Fig. 8 DIR of cylindrical shell panel $[0/90]_4$ utilizing C-3 end condition with $a/h=20$ and $\mu_s=0.1$ under uniform in-plane loading a Model I b Model II

the curvature ratio increases, there is a significant shift in dynamic instability towards lower frequencies range of excitation. The observation highlights the intricate and complex dynamics inherent in the behaviour of curved shell structures under these conditions. Also, the shell structure (G-3) exhibits a relatively high excitation frequency at a lower curvature ratio.

Effect of Support Conditions

This investigation focused on the behaviour of G-2 shell structure on NDEF responses subjected to different boundary conditions (Fig. 4). The geometrical parameters used as $a_1=a_2=1$, $r/a_1=40$, $a_1/h=200$ and $\alpha=0.1$. The consequences obtained from Models I and II are shown in Fig. 10 for various end restrictions. The C-6 end condition exhibits a straight-line instability region, while C-1 has a widespread region. Also, the shell structure exhibits a relatively high excitation frequency for Model II compared

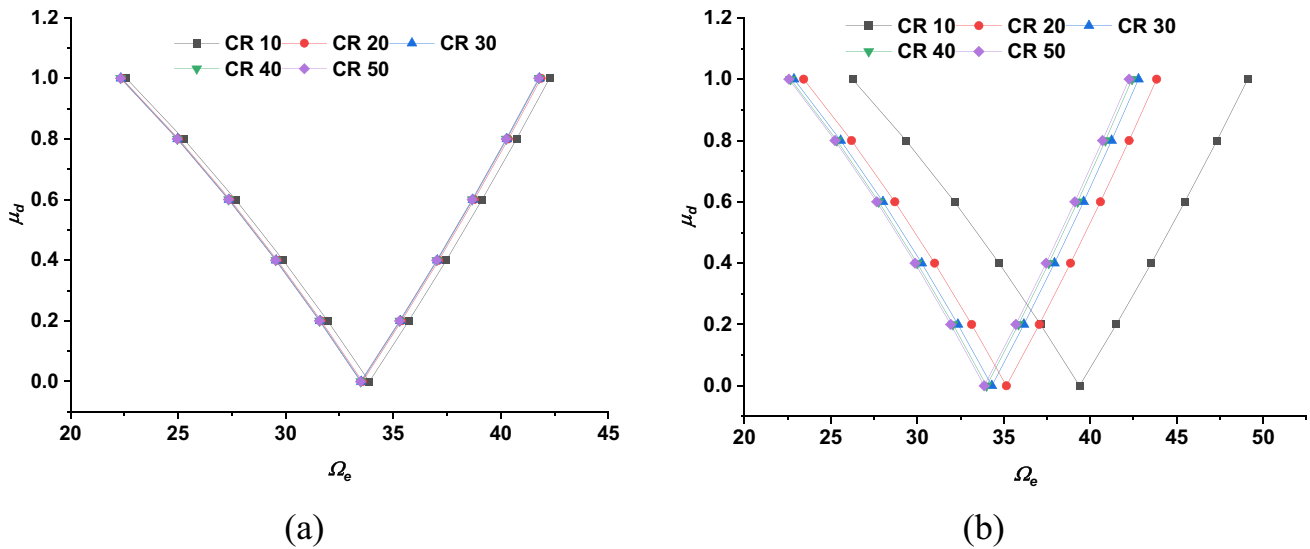


Fig. 9 DIR of spherical shell panel [0/90]₄ utilizing C-3 end condition with $a_1/h=20$ and $\mu_s=0.1$ under uniform in-plane loading **a** Model I **b** Model II

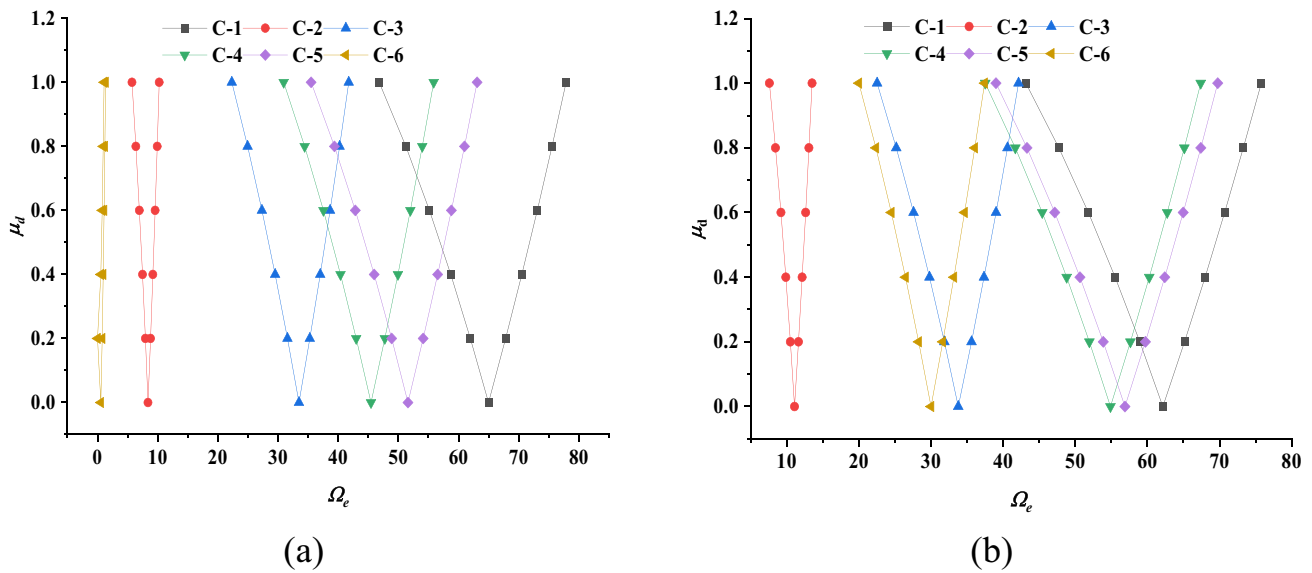


Fig. 10 Influence of support conditions on DIR of a [0/90]₄ laminated G-2 shell structure with $a_1=a_2=1$, $r/a_1=40$, $a_1/h=20$ and $\mu_s=0.1$ **a** Model I **b** Model II

to Model I. In contrast, it is the reverse for the C-1 end condition. These insights enhanced the understanding of how cylindrical shells respond under varied boundary conditions.

Effect of Thickness Ratio

The cylindrical shell panel with layup sequence (0/90)₄ having different thickness ratios has been considered for NDEF

responses with the geometrical parameters as $a_1=a_2=1$, $r/a_1=40$, and $\alpha=0.1$. Figure 11 depicts the results derived from Models I and II under various thickness ratios for the C-3 end condition. It is noteworthy from the figure that the increase in thickness ratio shifted the dynamic instability region to higher values of excitation frequency with the widespread region. However, this effect is less visible in Model I than in Model II. Model II shows a different trend of slight variation in dynamic instability region owing to higher stiffness with increased thickness ratios. The prominent

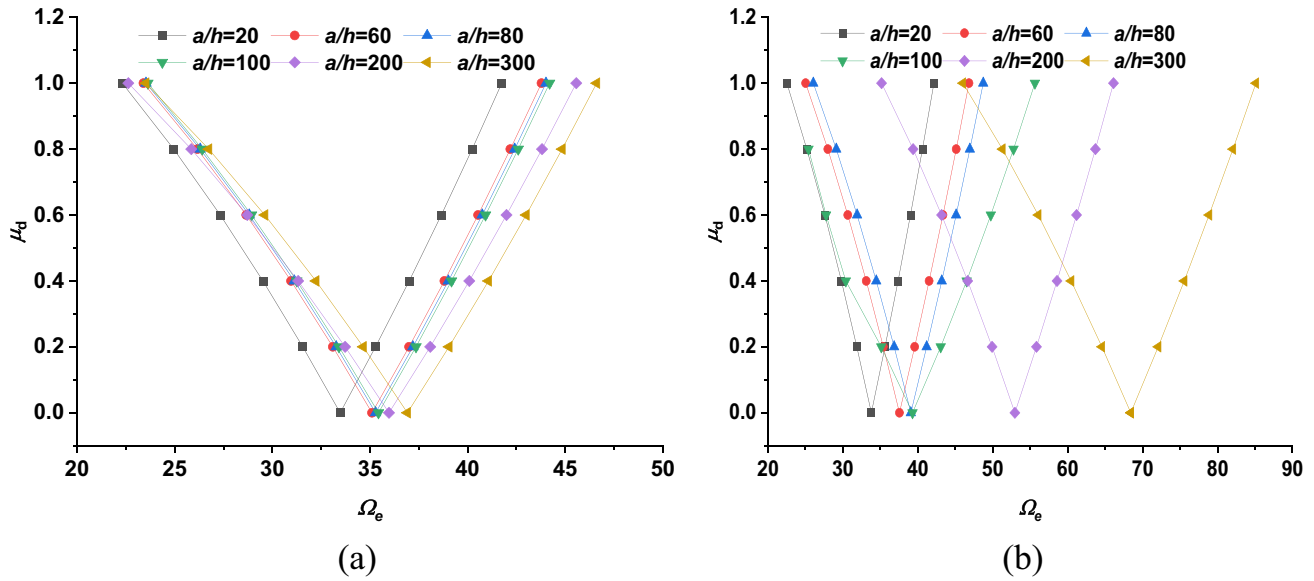


Fig. 11 Effect of thickness ratio on a $[0/90]_4$ laminated G-2 structure with $a_1 = a_2 = 1$ and $r/a_1 = 40$ a Model I b Model II

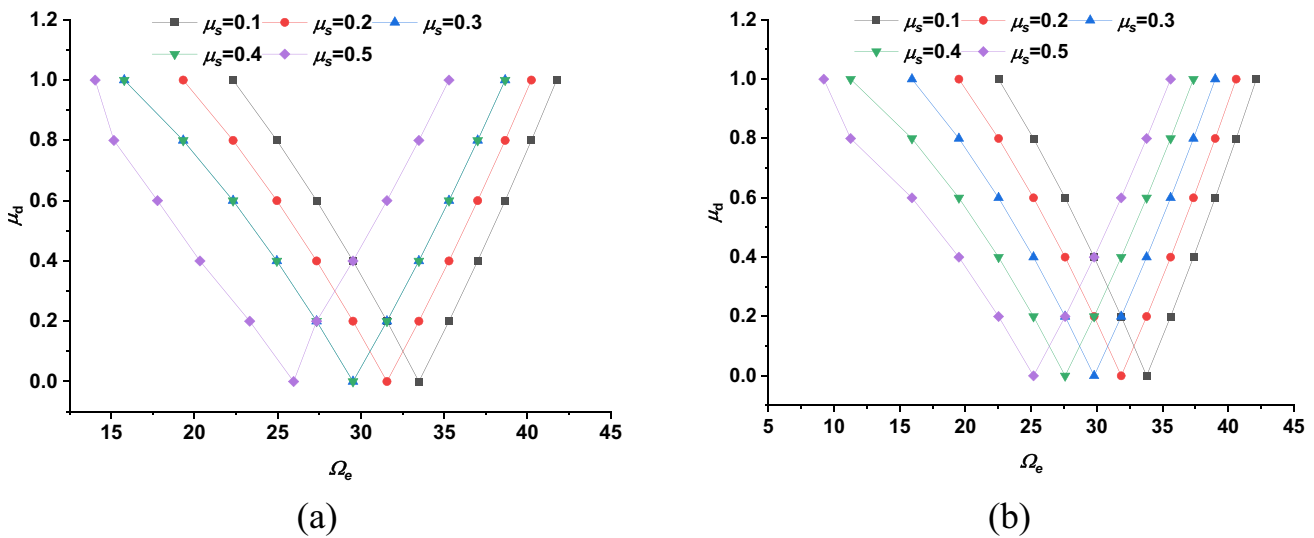


Fig. 12 DIR of a G-2 laminated structure $[0/90]_4$ with $a_1 = a_2 = 1$, $r/a_1 = 40$ and $a_1/h = 20$ subjected to different static load factors under uniform in-plane loading a Model I b Model II

effect on results is observed due to the inclusion of extra strain terms in the thickness direction of Model II.

Effect of Load Factor

In this illustration, the effect of various dynamic and static load factors on the NDEF responses of the G-2 shell structure ($a_1/h = 20$, $r/a_1 = 40$) has been investigated utilizing the C-3 end condition. The geometric and elastic properties remain the same as in the preceding section. Figure 12a, b demonstrate the findings from Models I and II,

respectively. The origin point of excitation frequency rises with a decrease in static load factor. However, the excitation frequency values obtained from Model II are slightly higher than those obtained from Model I. The shell structure shows high stiffness at low static load factors. One possible reason for the cause is amplification of dynamic responses at high static load factor, and ultimately triggering instability in both models considered at low excitation frequency.

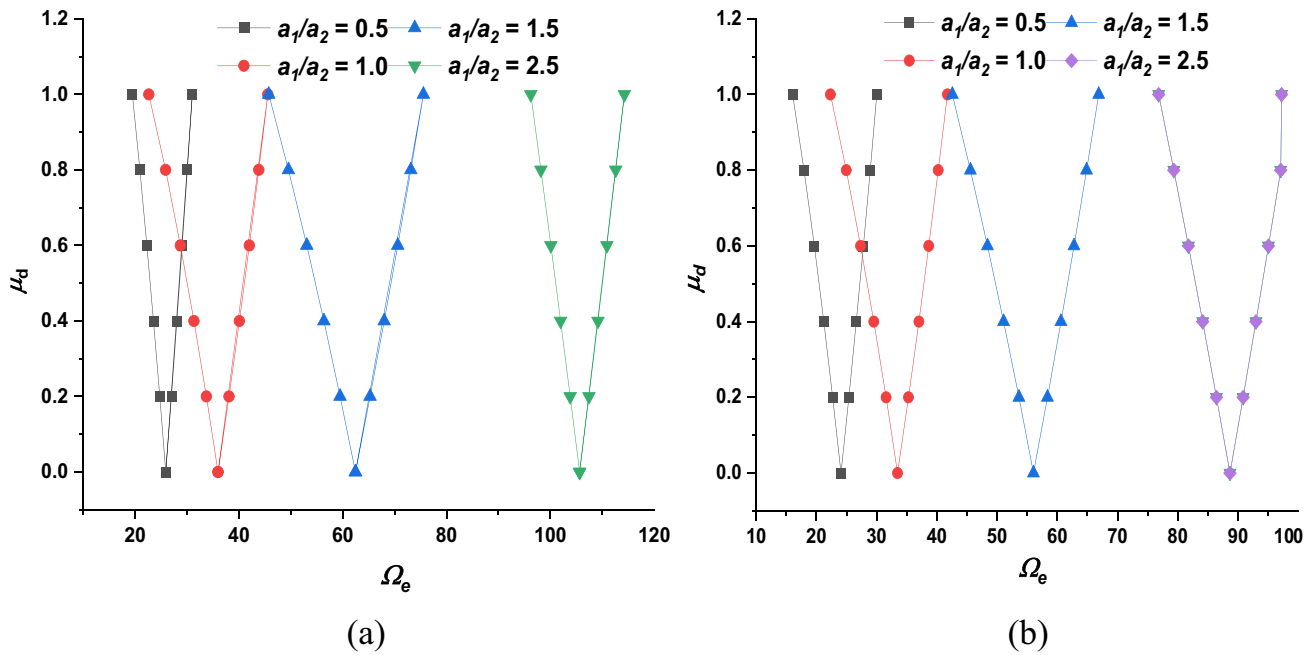


Fig. 13 Effect of aspect ratios on DIR of a $[0/90]_4$ laminated G-2 shell structure with $ra_1=40$, $a_1/h=20$ and $\mu_s=0.1$ **a** Model I **b** Model II

Effect of Aspect Ratio (AR)

The nuanced influence of varying AR ($a_1=1$ m and $a_2=2, 1, 0.67, 0.5, 0.4$) on the excitation frequency responses of a laminated structure is investigated utilizing C-3 end condition and presented in Fig. 13. The aspect ratio of 1.5 gave the widest instability region. The Ω_e rises with an upsurge in AR. The region of instability expands with the increase in AR up to the optimum value; after that, it decreases further.

Conclusion

The parametric excitation frequency characteristics of laminated curved shell structure under in-plane loading are provided in a general framework utilizing two different higher-order models. The numerical results are obtained using isoparametric FE steps based on the Bolotin approach. The numerical predictions made with the FEM model agree well with the excitation frequencies of the flat composite plates. Further, the influence of various models and input parameters are pondered in the succeeding lines:

- The dynamic instability of the curved composite structure occurs at a higher Ω_e for the increased thickness ratio. Also, the instability region expands with an increase in the thickness ratio.
- The curved shell structure exhibits higher stiffness than the flat plate structure. The dynamic instability ori-

gin point increases with the aspect and curvature ratio increase.

- The instability region widens and shifts to lower disturbing frequencies as the static load factor increases, destabilizing the dynamic stability behaviour of the composite structure.
- The Ω_e values increase with an increase in end restriction. The C-1 end condition exhibits the highest Ω_e values. Model II exhibits higher instability origin point values for various end conditions except C-1.
- Model II exhibits somewhat more precision than Model I due to the negligence of some strain terms in Model I.

It can be seen from the consequences that the geometry shape, curvature, span length and dynamic and static load factor all affect the stability of the composite structure. As a result, while working with structures that are exposed to in-plane loads, the designer must exercise caution. This research has additional applications in monitoring structural health when designing a laminated curved composite for construction.

Data Availability All data utilized/computed are already within the text. If anything, extra required can be provided on reasonable request.

Declarations

Conflict of Interest On behalf of all authors, the corresponding author states that there is no conflict of interest.

References

1. Türkmen HS, Mecitoğlu Z (1999) dynamic response of a stiffened laminated composite plate subjected to blast load. *J Sound Vib* 221:371–389. <https://doi.org/10.1006/jsvi.1998.1976>
2. Uyaner M, Kara M (2007) Dynamic response of laminated composites subjected to low-velocity impact. *J Compos Mater* 41:2877–2896. <https://doi.org/10.1177/0021998307079971>
3. Tanveer M, Singh AV (2009) Linear and nonlinear dynamic responses of various shaped laminated composite plates. *J Comput Nonlinear Dyn* 4:1–13. <https://doi.org/10.1115/1.3187177>
4. Wang Z, Liang X, Fallah AS et al (2013) A novel efficient method to evaluate the dynamic response of laminated plates subjected to underwater shock. *J Sound Vib* 332:5618–5634. <https://doi.org/10.1016/j.jsv.2013.05.028>
5. Civalek Ö (2013) Composites : Part B Nonlinear dynamic response of laminated plates resting on nonlinear elastic foundations by the discrete singular convolution-differential quadrature coupled approaches h. *Compos Part B* 50:171–179. <https://doi.org/10.1016/j.compositesb.2013.01.027>
6. Nguyen-Quang K, Vo-Duy T, Dang-Trung H, Nguyen-Thoi T (2018) An isogeometric approach for dynamic response of laminated FG-CNT reinforced composite plates integrated with piezoelectric layers. *Comput Methods Appl Mech Eng* 332:25–46. <https://doi.org/10.1016/j.cma.2017.12.010>
7. Adhikari B, Singh BN (2018) An efficient higher order non-polynomial Quasi 3-D theory for dynamic responses of laminated composite plates. *Compos Struct* 189:386–397. <https://doi.org/10.1016/j.compstruct.2017.10.044>
8. Gliszczynski A, Kubiak T, Rozylo P et al (2019) The response of laminated composite plates and profiles under low-velocity impact load. *Compos Struct* 207:1–12. <https://doi.org/10.1016/j.compsstruct.2018.09.005>
9. Zhang P, Qi C, Fang H et al (2019) Semi-analytical analysis of static and dynamic responses for laminated magneto-electro-elastic plates. *Compos Struct* 222:110933. <https://doi.org/10.1016/j.compstruct.2019.110933>
10. Parida SP, Jena PC (2023) Selective layer-by-layer fillering and its effect on the dynamic response of laminated composite plates using higher-order theory. *J Vib Control* 29:2473–2488. <https://doi.org/10.1177/10775463221081180>
11. Loughlan J (1999) The influence of bend–twist coupling on the shear buckling response of thin laminated composite plates. *Thin-Walled Struct* 34:97–114. [https://doi.org/10.1016/S0263-8231\(99\)00009-9](https://doi.org/10.1016/S0263-8231(99)00009-9)
12. Weaver PM, Nemeth MP (2007) Bounds on flexural properties and buckling response for symmetrically laminated composite plates. *J Eng Mech* 133:1178–1191. [https://doi.org/10.1061/\(ASCE\)0733-9399\(2007\)133:11\(1178\)](https://doi.org/10.1061/(ASCE)0733-9399(2007)133:11(1178))
13. Baba BO, Baltacı A (2007) Buckling characteristics of symmetrically and antisymmetrically laminated composite plates with central cutout. *Appl Compos Mater* 14:265–276. <https://doi.org/10.1007/s10443-007-9045-z>
14. Baba BO (2007) Buckling behavior of laminated composite plates. *J Reinf Plast Compos* 26:1637–1655. <https://doi.org/10.1177/0731684407079515>
15. Dash P, Singh BN (2014) Buckling and post-buckling response of laminated composite plate with random system properties. *Mech Adv Mater Struct* 21:516–529. <https://doi.org/10.1080/15376494.2012.699597>
16. Singh BN, Lal A, Kumar R (2009) Post buckling response of laminated composite plate on elastic foundation with random system properties. *Commun Nonlinear Sci Numer Simul* 14:284–300. <https://doi.org/10.1016/j.cnsns.2007.08.005>
17. Shi P, Dong C, Sun F et al (2018) A new higher order shear deformation theory for static, vibration and buckling responses of laminated plates with the isogeometric analysis. *Compos Struct* 204:342–358. <https://doi.org/10.1016/j.compstruct.2018.07.080>
18. Patel SN, Sheikh AH (2016) Buckling response of laminated composite stiffened plates subjected to partial in-plane edge loading. *Int J Comput Methods Eng Sci Mech* 17:322–338. <https://doi.org/10.1080/15502287.2016.1231235>
19. Nguyen PD, Papazafeiropoulos G, Vu Q-V, Duc ND (2022) Buckling response of laminated FG-CNT reinforced composite plates: analytical and finite element approach. *Aerosp Sci Technol* 121:107368. <https://doi.org/10.1016/j.ast.2022.107368>
20. Singh SK, Chakrabarti A (2012) Buckling analysis of laminated composite plates using an efficient C0 FE model. *Lat Am J Solids Struct* 9:1–13. <https://doi.org/10.1590/S1679-7825201200030003>
21. Balamurugan V, Ganapathi M, Varadan TK (1996) Nonlinear dynamic instability of laminated composite plates using finite element method. *Comput Struct* 60:125–130. [https://doi.org/10.1016/0045-7949\(95\)00368-1](https://doi.org/10.1016/0045-7949(95)00368-1)
22. Ganapathi M, Balamurugan V (1998) Dynamic instability analysis of a laminated composite circular cylindrical shell. *Comput Struct* 69:181–189. [https://doi.org/10.1016/S0045-7949\(98\)00095-9](https://doi.org/10.1016/S0045-7949(98)00095-9)
23. Kumar LR, Datta PK, Prabhakara DL (2003) Dynamic instability characteristics of laminated composite plates subjected to partial follower edge load with damping. *Int J Mech Sci* 45:1429–1448. <https://doi.org/10.1016/j.ijmecsci.2003.10.008>
24. Patel SN, Datta PK, Sheikh AH (2009) Parametric study on the dynamic instability behavior of laminated composite stiffened plate. *J Eng Mech* 135:1331–1341. [https://doi.org/10.1061/\(asce\)0733-9399\(2009\)135:11\(1331\)](https://doi.org/10.1061/(asce)0733-9399(2009)135:11(1331))
25. Fayaz D, Patel SN, Kumar R, Watts G (2023) Nonlinear dynamic instability of laminated composite stiffened plates subjected to in-plane pulsating loading. *Mech Adv Mater Struct*. <https://doi.org/10.1080/15376494.2023.2216692>
26. Darabi M, Ganesan R (2018) Nonlinear dynamic instability analysis of laminated composite thin plates subjected to periodic in-plane loads. *Nonlinear Dyn* 91:187–215. <https://doi.org/10.1007/s11071-017-3863-9>
27. Sahoo R, Singh BN (2018) Assessment of dynamic instability of laminated composite-sandwich plates. *Aerosp Sci Technol* 81:41–52. <https://doi.org/10.1016/j.ast.2018.07.041>
28. Huynh HQ, Nguyen H, Nguyen HLT (2017) Non-linear parametric vibration and dynamic instability of laminated composite plates using extended dynamic stiffness method. *J Eng Technol* 6:170–185
29. Sahoo R, Singh BN (2015) Dynamic instability of laminated-composite and sandwich plates using a new inverse trigonometric zigzag theory. *J Vib Acoust Trans ASME* 137:1–12. <https://doi.org/10.1115/1.4030716>
30. Chattopadhyay A, Radu AG (2000) Dynamic instability of composite laminates using a higher order theory. *Comput Struct* 77:453–460. [https://doi.org/10.1016/S0045-7949\(00\)00005-5](https://doi.org/10.1016/S0045-7949(00)00005-5)
31. Sahoo S, Parida SP, jena PC, (2023) Dynamic response of a laminated hybrid composite cantilever beam with multiple cracks & moving mass. *Struct Eng Mech* 87:529–540. <https://doi.org/10.12989/sem.2023.87.6.529>
32. Sahoo S, Jena PC (2022) Preparation and characterization of hybrid laminated composite beams. *Adv Mater Process Technol* 8:899–912. <https://doi.org/10.1080/2374068X.2021.1953924>
33. Sahoo S, Jena PC (2023) Effect of lamina orientation, crack severity, and fillers on dynamic parameters of hybrid composite cantilever beam with double transverse cracks. *Materwiss Werkstech* 54:737–750. <https://doi.org/10.1002/mawe.202200205>

34. Parida SP, Jena PC (2022) Multi-fillers GFRP laminated composite plates: fabrication & properties. *Indian J Eng Mater Sci* 29:815–823. <https://doi.org/10.56042/ijems.v29i6.70296>
35. Parida SP, Jena PC (2020) Advances of the shear deformation theory for analyzing the dynamics of laminated composite plates: an overview. *Mech Compos Mater* 56:455–484. <https://doi.org/10.1007/s11029-020-09896-0>
36. Parida SP, Jena PC (2022) Free and forced vibration analysis of flyash/graphene filled laminated composite plates using higher order shear deformation theory. *Proc Inst Mech Eng Part C J Mech Eng Sci* 236:4648–4659. <https://doi.org/10.1177/09544062211053181>
37. Parida SP, Jena PC, Dash RR (2019) FGM Beam analysis in dynamical and thermal surroundings using finite element method. *Mater Today Proc* 18:3676–3682. <https://doi.org/10.1016/j.matpr.2019.07.301>
38. Parida SP, Jena PC, Dash RR (2023) Dynamics of rectangular laminated composite plates with selective layer-wise fillering rested on elastic foundation using higher-order layer-wise theory. *JVC/J Vib Control* 29:5598–5615. <https://doi.org/10.1177/10775463221138353>
39. Parida SP, Jena PC, Das SR et al (2022) Comparative stress analysis of different suitable biomaterials for artificial hip joint and femur bone using finite element simulation. *Adv Mater Process Technol* 8:1741–1756. <https://doi.org/10.1080/2374068X.2021.1949541>
40. Pradhan S, Das SR, Jena PC, Dhupal D (2022) Investigations on surface integrity in hard turning of functionally graded specimen under nano fluid assisted minimum quantity lubrication. *Adv Mater Process Technol* 8:1714–1729. <https://doi.org/10.1080/2374068X.2021.1948706>
41. Pradhan S, Das SR, Jena PC, Dhupal D (2022) Machining performance evaluation under recently developed sustainable HAJM process of zirconia ceramic using hot SiC abrasives: an experimental and simulation approach. *Proc Inst Mech Eng Part C J Mech Eng Sci* 236:1009–1035. <https://doi.org/10.1177/09544062211010199>
42. Bin ZF, Ong ZC, Khoo SY (2020) A review of operational modal analysis techniques for in-service modal identification. *J Brazilian Soc Mech Sci Eng*. <https://doi.org/10.1007/s40430-020-02470-8>
43. Varma PCR, Colreavy J, Cassidy J et al (2009) Effect of organic chelates on the performance of hybrid sol-gel coated AA 2024–T3 aluminium alloys. *Prog Org Coatings* 66:406–411. <https://doi.org/10.1016/j.porgcoat.2009.09.004>
44. Jena PC, Parhi DR, Pohit G (2016) Dynamic study of composite cracked beam by changing the angle of bidirectional fibres. *Iran J Sci Technol Trans A Sci* 40:27–37. <https://doi.org/10.1007/s40995-016-0006-y>
45. Jena PC (2018) Fault assessment of FRC cracked beam by using neuro-fuzzy hybrid technique. *Mater Today Proc* 5:19216–19223. <https://doi.org/10.1016/j.matpr.2018.06.277>
46. Charan Jena P, Parida SP, Dash RR (2018) Modal study of trapezoidal cantilever plate like composite beam. *Mater Today Proc* 5:19680–19692. <https://doi.org/10.1016/j.matpr.2018.06.330>
47. Charan Jena P (2018) Identification of crack in sic composite polymer beam using vibration signature. *Mater Today Proc* 5:19693–19702. <https://doi.org/10.1016/j.matpr.2018.06.331>
48. Jena PC, Parhi DR, Pohit G, Samal BP (2015) Crack assessment by FEM of AMMC beam produced by modified stir casting method. *Mater Today Proc* 2:2267–2276. <https://doi.org/10.1016/j.matpr.2015.07.263>
49. Jena PC, Parhi DR, Pohit G (2019) Dynamic investigation of FRP cracked beam using neural network technique. *J Vib Eng Technol* 7:647–661. <https://doi.org/10.1007/s42417-019-00158-5>
50. Jena PC, Parhi DR, Pohit G (2014) Theoretical, numerical (FEM) and experimental analysis of composite cracked beams of different boundary conditions using vibration mode shape curvatures. *Int J Eng Technol* 6:509–518
51. Jena PC (2018) Free vibration analysis of short bamboo fiber based polymer composite beam structure. *Mater Today Proc* 5:5870–5875. <https://doi.org/10.1016/j.matpr.2017.12.185>
52. Li H, Liu Y, Zhang H et al (2023) Amplitude-dependent damping characteristics of all-composite sandwich plates with a foam-filled hexagon honeycomb core. *Mech Syst Signal Process* 186:109845. <https://doi.org/10.1016/j.ymsp.2022.109845>
53. Liu Yf, Qin Zy, Chu Fl (2022) Nonlinear free vibration of graphene platelets reinforced composite corrugated plates. *J Cent South Univ* 29:3054–3064. <https://doi.org/10.1007/s11771-022-5086-6>
54. Zhu R, Zhang X, Zhang S et al (2022) Modeling and topology optimization of cylindrical shells with partial CLD treatment. *Int J Mech Sci* 220:107145. <https://doi.org/10.1016/j.ijmecsci.2022.107145>
55. Liu Y, Qin Z, Chu F (2021) Nonlinear forced vibrations of FGM sandwich cylindrical shells with porosities on an elastic substrate. *Nonlinear Dyn* 104:1007–1021. <https://doi.org/10.1007/s11071-021-06358-7>
56. Liu Y, Qin Z, Chu F (2021) Nonlinear dynamic responses of sandwich functionally graded porous cylindrical shells embedded in elastic media under 1:1 internal resonance. *Appl Math Mech Eng Ed* 42:805–818. <https://doi.org/10.1007/s10483-021-2740-7>
57. Qin Z, Zhao S, Pang X et al (2020) A unified solution for vibration analysis of laminated functionally graded shallow shells reinforced by graphene with general boundary conditions. *Int J Mech Sci* 170:105341. <https://doi.org/10.1016/j.ijmecsci.2019.105341>

Publisher's Note Springer Nature remains neutral with regard to jurisdictional claims in published maps and institutional affiliations.

Springer Nature or its licensor (e.g. a society or other partner) holds exclusive rights to this article under a publishing agreement with the author(s) or other rightsholder(s); author self-archiving of the accepted manuscript version of this article is solely governed by the terms of such publishing agreement and applicable law.